Proc. TSF1 1977, Springer 1979

Direct Numerical Simulation of Turbulent Velocity, Pressure, and Temperature Fields in Channel Flows

G. Grötzbach and U. Schumann

Kernforschungszentrum Karlsruhe, Institut für Reaktorentwicklung
Postfach 3640, D-7500 Karlsruhe, Fed. Rep. of Germany

Abstract

A finite difference scheme for direct numerical simulation of turbulent velocity, pressure, and temperature fields in plane channels and annuli is described. The fluid is incompressible and has constant density and diffusivities. The method is an extended and revised version of an earlier one. It now includes simultaneous simulation of the temperature field and employs a revised subgrid scale model which has been extended to allow for moderately high Reynolds numbers (Re > 10,000) and poorly resolving grids. The purpose of this paper is to report and demonstrate the improved capabilities of the method.

Nomenclature

a	Dimensionless conductivity (= $1/\mathrm{Pe}_\tau$)	T	Temperature
a_t	SGS turbulent conductivity	u_i	Velocity components
c	SGS model coefficient	u_b	Bulk velocity
D	Distance between the walls	u_0	Wall shear-stress velocity
${}^jF$	Grid cell surface with normal in x_j-direction	x_i	Coordinates, see Fig. 1
		ν	Kinematic viscosity (= $1/\mathrm{Re}_\tau$)
		σ	Correction factor
IM, JM, KM	Number of grid cell in x_1-, x_2-, x_3-direction	τ_w	Wall shear stress
		$\hat{y}$	Any dimensionfull quantity y
h	Grid spacing $(\Delta x_1 \cdot \Delta x_2 \cdot \Delta x_3)^{1/3}$	y'	Fluctuating part
p	Kinematic pressure	$\langle y \rangle$	Time mean value
$\dot{q}_w$	Wall heat flux	$\overline{v}^{\overline{y}}$	Grid volume mean value
R_1/R_2	Inner/outer radius	${}^j\overline{y}$	Surface mean value (taken over ${}^jF$)
t	Time	rms	Root time mean square value

Introduction

Direct numerical simulation of turbulent flows is a new important tool to study the basic properties of turbulence. Here, we describe an improved and extended finite difference simulation of turbulent flows in plane channels and annuli. The geometry is shown in Fig. 1. The scheme is designed for Reynolds numbers

$$\mathrm{Re} = \hat{u}_b \hat{D}/\hat{\nu} > 10{,}000 \qquad (1)$$

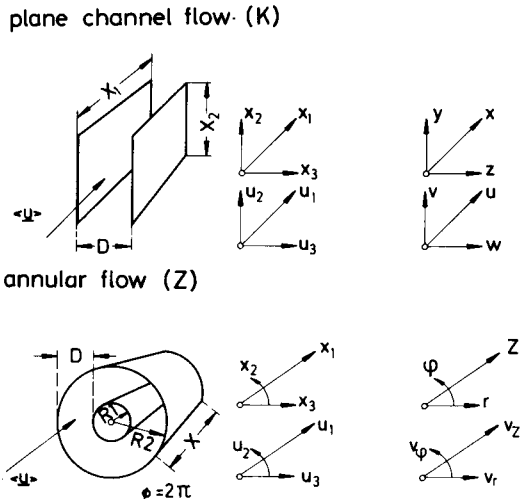

Fig. 1. Channel geometry

In this stage we restrict ourselves to nonbuoyant flows with constant viscosity ν and conductivity a so that the temperature is a passive scalar. The direct numerical simulation describes the time-dependent and three-dimensional large-scale turbulence under statistically steady-state conditions. The large scales are those which are resolved by the three-dimensional grid of the finite-difference scheme. Typically up to 32 grid points can be used in each direction. The effect of the subgrid scale (SGS) motion is accounted for by a SGS model. This approach has been developed by *Deardorff* [1] and others and formed the basis of the code TURBIT-1 [2, 3] ("*TURB*ulenter *I*mpuls *T*ransport").

Further investigations have been concentrating on the following items [4]:

- development of a code TURBIT-2 for simultaneous simulation of turbulent temperature fields in addition to velocity and pressure fields for plane channels and annuli.
- extension of the SGS model for SGS temperature transport and improvement of the existing models in order to allow for a wider range of Reynolds numbers (from moderate to very high) and to get reasonable results even on very coarse grids (which reduce the necessary computing time).
- verification of the accuracy of the temperature simulation by comparison with experiments.

As a result, TURBIT-2 has been established, and several cases have been run in order to study the effect of the improved SGS model. For this purpose we used between 2048 and 32768 grid cells. The present code is capable of larger grids; however, the computing time required to attain steady state conditions becomes prohibitive long for more grid points; in earlier studies a grid with 32 x 32 x 64 = 65576 points has been used [2]. In the following we give some details of the method, summarize the experiences got up to now, and present some results obtained with respect to the temperature simulation.

The Method Used in Turbit-2

Finite Difference Scheme

The code TURBIT-2 is based on a finite difference scheme which approximates the Navier-Stokes equation, the continuity and the temperature equation. For the deduction of this scheme the basic equations are averaged over finite grid volumes as described in [2]. Hereby,

the triple integral defining the average is integrated by parts with respect to the divergence-type terms so that the average is expressed in terms of finite differences of surface mean values. This allows us to account for anisotropies introduced by grid cells with different spacings Δx_i and by cylindrical coordinates. The nomenclature is as follows:

$\delta_j y$ finite difference operator applied to some space function y, e.g.,

$$\delta_1 y = \frac{1}{\Delta x_1}[y(x_1 + \Delta x_1/2, x_2, x_3) - y(x_1 - \Delta x_1/2, x_2, x_3)] \tag{2}$$

${}^{j}\overline{y}$ surface mean value, e.g.,

$$1\overline{Y} = \frac{1}{\Delta x_2 \Delta x_3} \int_{\Delta x_2} \int_{\Delta x_3} y(x_1, z_2, z_3)\, dz_3 dz_2 \tag{3}$$

${}^{v}\overline{y}$ volume mean value

$${}^{v}\overline{y} = \frac{1}{\Delta x_1 \Delta x_2 \Delta x_3} \int_{\Delta x_1} \int_{\Delta x_2} \int_{\Delta x_3} y(z_1, z_2, z_3) \cdot dz_3 dz_2 dz_1 . \tag{4}$$

The resultant equations are the

– averaged momentum (Navier-Stokes) equation

$$\frac{\partial}{\partial t}\,{}^{v}\overline{u_i} + \delta_j({}^{j}\overline{u_j u_i}) = -\delta_i\,{}^{i}\overline{p} + \delta_j\left(\nu\,{}^{j}\overline{\frac{\partial u_i}{\partial x_j}}\right) + \delta_{i1} P_x \tag{5}$$

– averaged mass (continuity) equation

$$\delta_i\,{}^{i}\overline{u_i} = 0 \tag{6}$$

– averaged temperature equation

$$\frac{\partial}{\partial t}\,{}^{v}\overline{T} + \delta_j({}^{j}\overline{u_j T}) = \delta_j\left(a\,{}^{j}\overline{\frac{\partial T}{\partial x_j}}\right) + {}^{v}\overline{Q}. \tag{7}$$

The summation convention is assumed[1]. All quantities are made dimensionless by means of the length scale $\hat{D}$, the friction velocity $\hat{u}_0 = (\hat{\tau}_0/\hat{\rho}_0)^{1/2}$ ($\hat{\tau}_0$ = time mean wall shear stress averaged over both walls, $\hat{\rho}_0$ = constant density), and the heat-flux temperature $\hat{T}_0 = \hat{q}_0/[\hat{\rho}\hat{c}\hat{u}_0]$ ($\hat{q}_0$ = time mean wall heat flux, $\hat{c}$ = specific heat capacity). The dimensionless diffusivities are $\nu = \hat{\nu}/(\hat{u}_0\hat{D})$ and $a = \hat{a}/(\hat{u}_0\hat{D})$. The common Reynolds number Re and the friction coefficient c_f are related to $\mathrm{Re}_\tau = 1/\nu$ by

$$\mathrm{Re}_\tau = \mathrm{Re}\,(\hat{u}_0/\hat{u}_b) = \mathrm{Re}\sqrt{c_f/8} \tag{8}$$

The mean pressure gradient or driving force $P_x = 2$ is introduced so that the fluctuating pressure field p has a zero mean gradient in the axial direction. We assume that the axial mean temperature gradient is zero, too. Otherwise a transformation has to be used as given in [4], p. 65.

[1] Fór repeated lower indices.

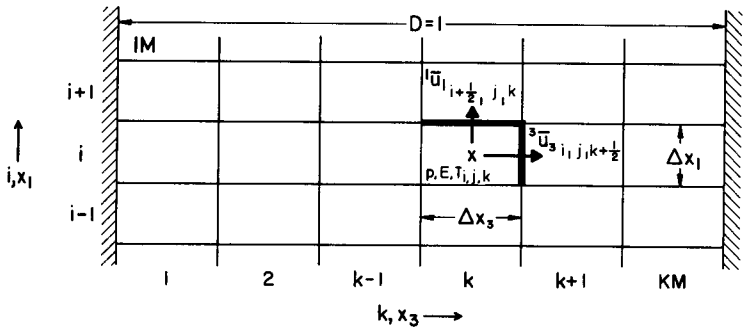

Fig. 2. Staggered grid

The averaged products can be rewritten as

$$^{j}\overline{u_i u_j} = {}^{j}\bar{u}_i\,{}^{j}\bar{u}_j + {}^{j}\overline{u_i' u_j'} \tag{9}$$

$$^{j}\overline{u_j T} = {}^{j}\bar{u}_j\,{}^{j}\bar{T} + {}^{j}\overline{u_j' T'} \tag{10}$$

where $u_i' = u_i - {}^{j}\bar{u}_i$, $T' = T - {}^{j}\bar{T}$. The second part of each sum forms the SGS fluxes.

So far, no approximations have been involved. Indeed, Eqs. (5)–(7) are the conservation laws written in their integral form for grid volumes. However, the equations are as yet unclosed. The next step, therefore, is to express all quantities in terms of grid quantities. We employ a staggered grid as shown in Fig. 2. This allows us to retain the continuity equation in its exact form, Eq. (6). The quantities not defined on the grid are approximated in a linear and second-order manner using algebraic averages like $\bar{y}^{j}$, e.g.,

$$\bar{y}^{1} = \tfrac{1}{2}\,[y(x_1 + \Delta x_1/2, x_2, x_3) + y(x_1 - \Delta x_1/2, x_2, x_3)]. \tag{11}$$

This results in the following finite difference scheme which we write without space averaging bars; the superscript n refers to the time level ($t^n = n\Delta t$):

$$(\tilde{u}_i^{n+1} - u_i^{n-1})/(2\Delta t) = -\delta_j(\bar{u}_j^{i}\bar{u}_i^{j})^{n} + \delta_j(\nu\delta_j u_i - {}^{j}\overline{u_i' u_j'})^{n-1} + \delta_{i1}P_x \tag{12}$$

$$(T^{n+1} - T^{n-1})/(2\Delta t) = -\delta_j(u_j\bar{T}^{j})^{n} + \delta_j(a\delta_j T - {}^{j}\overline{u_j' T'})^{n-1} + \dot{Q}^{n}. \tag{13}$$

The pressure p^n is determined from a Poisson equation

$$\delta_i\delta_i p^n = \delta_i\tilde{u}_i^{n+1}/(2\Delta t) \tag{14}$$

so that the new time level velocities

$$u_i^{n+1} = \tilde{u}_i^{n+1} - (2\Delta t)\,\delta_i p^n \tag{15}$$

satisfy the continuity equation (6). Equation (14) is solved using fast Fourier transform [5]. Equations (12) and (13) correspond to a leap frog scheme which is started with an initial Euler step and interrupted by an averaging step every n_L time steps (typically, $n_L = 50$). The actual code can be applied also for cylindrical coordinates and nonequidistant grid spacings in the x_3-direction.

The Subgrid Scale Flux Approximations

The general form of the model for the SGS stresses ${}^{j}\overline{u_i' u_j'}$ is as described in [2]; several improvements have been added [4], however. The SGS heat flux ${}^{j}\overline{u_i' T'}$ has been modeled in an analogous manner [4]. The main characteristics are as follows.

First, the SGS fluxes are split into a fluctuating and a time mean part, e.g.,

$$\underbrace{{}^{j}\overline{u_j' T'}}_{\text{"locally isotropic part"}} = \underbrace{{}^{j}\overline{u_j' T'} - \langle {}^{j}\overline{u_j' T'} \rangle}_{\text{"locally isotropic part"}} + \underbrace{\langle {}^{j}\overline{u_j' T'} \rangle}_{\text{"inhomogeneous part"}} \tag{16}$$

and approximated by eddy diffusivity models

$${}^{j}\overline{u_j' T'} = -{}^{j}a_t \delta_j ({}^{v}\overline{T} - \langle {}^{v}\overline{T} \rangle) - {}^{j}a_t^x \delta_j \langle {}^{v}\overline{T} \rangle \tag{17}$$

$${}^{j}a_t = c_{T2}\, {}^{j}c_T ({}^{j}F\, {}^{j}c_5\, {}^{v}\overline{E'})^{1/2}/\sigma_T \tag{18}$$

$${}^{j}a_t^x = \delta_{3j} \ell \ell_H |\delta_3 \langle {}^{1}\bar{u}_1 \rangle| f_H \text{ (mesh)}. \tag{19}$$

The corresponding eddy diffusivities [2] of the SGS stresses are

$${}^{ij}\mu = c_2\, {}^{ij}c ({}^{j}F\, {}^{j}c_5\, {}^{v}\overline{E'})^{1/2}/\sigma_1 \tag{20}$$

$${}^{ij}\mu^x = \delta_{i1}\delta_{j3} \ell^2 |\delta_3 \langle {}^{1}\bar{u}_1 \rangle| f \text{ (mesh)}. \tag{21}$$

The "*isotropic*" *eddy diffusivities* ${}^{j}a_t$ and ${}^{ij}\mu$ are determined under the assumption of locally isotropic turbulence. Here, the characteristic length scale is derived from the surface area ${}^{j}F$ of the grid cell over which the average is defined and the characteristic velocity from the SGS kinetic energy ${}^{v}\overline{E'}$. The coefficients ${}^{j}c_5$, ${}^{ij}c$, ${}^{j}c_T$ [2, 4] account for geometrical details of the mesh and the finite difference scheme, and they are of order one. The coefficients c_2 and c_{T2}, however, must be determined so that the energy or temperature variance dissipation due to the eddy diffusivities in the simulated gross-scale flow is of the same magnitude as the molecular dissipation in reality. For this purpose we assume the validity of the well-known Kolmogorov-Spectrum for the kinetic energy $E(k)$ (k = wave number) and its counterpart for temperature $E_T(k)$:

$$E(k) = a \langle \epsilon \rangle^{2/3} k^{-5/3}, \quad E_T(k) = \beta \langle \epsilon \rangle^{-1/3} \langle \epsilon_T \rangle k^{-5/3} \tag{22}$$

$$\int_0^\infty E(k)dk = \tfrac{1}{2} \langle u_i'^2 \rangle, \quad \int_0^\infty E_T(k)dk = \langle T'^2 \rangle \tag{23}$$

$$\epsilon = \nu (\partial u_i / \partial x_k)^2, \quad \epsilon_T = 2a (\partial T / \partial x_k)^2. \tag{24}$$

According to several experiments [4] we assume the Kolmogorov- and Batchelor-constants α and β to be

$$\alpha = 1.5, \quad \beta = 1.3. \tag{25}$$

Table 1. SGS coefficients for an isotropic grid ($\Delta x_1 = \Delta x_2 = \Delta x_3 = 1/16$) (Re = 250,000, Pr = 0.7)

Stress model		Kinetic energy model		Heat-flux model	
c_2	0.0709	c_3	0.6336	c_{T2}	0.1807
${}^{j}c_5$	0.8283	c_{31}	0.74	${}^{j}c_T$	1.0
${}^{11}c$	1.4744	c_{32}	20.0	σ_T	1.4
${}^{12}c$	0.8233	c_{20}	0.8044	c_{T10}	1.0
c_{10}	2.0				
F_0	1.28				
σ_1	1.4				

By means of these assumptions all coefficients $c_2, c_{T2}, {}^{j}c_5, {}^{ij}c, {}^{j}c_T$ can be evaluated [2, 4] without further approximations. Nevertheless, in [4] we use the coefficients σ_T and σ_1 to adjust the models numero-empirically and to account for the deficiencies of the theory. The values of the coefficients, $c \ldots$, are dependent on the geometry of the mesh. Typical values of all SGS coefficients are listed in Table 1. The value of c_2 is different from that given in [2] which was erroneous due to a sign error in the underlying theory ([5, see 4]). This (and the changes in the energy equation, see below) result in a reduction of the factor σ_1 from 3 [2] to 1.4 [4]. The assumption of spectra of the Kolmogorov-type is not necessary. More realistic spectra which depart at small as well as at high wave numbers have also been used [4, 6]. The changes of c_2 introduced by these spectra remain less than 20% for the cases considered up to now. They become important, however, for fine grids and small Reynolds numbers, where the grid scale becomes comparable to the Kolmogorov microscale.

The *"inhomogeneous" eddy diffusivities* ${}^{j}a_t^x$ and ${}^{ij}\mu^x$ are derived from the common mixing length models (ℓ, ℓ_H = mixing lengths for momentum and heat [4]). The crucial factors here are the damping functions f and f_H. They are designed so that for very coarse meshes the SGS model becomes equal to the common models for time-averaged turbulence ($f, f_H \to 1$). For very fine resolution the functions go to zero since in this case all SGS fluxes are described by the isotropic parts. We use [4]:

$$f(\text{mesh}) = \min \{1, c_{10}[(\Delta x_1 \Delta x_2^2 \Delta x_3)/F_0^2]^{1/2}\} \tag{26}$$

$$f_H(\text{mesh}) = \min \{1, [c_{10} c_{T10} (\Delta x_1^2 \Delta x_2^2 \Delta x_3)^{2/5}/F_0]^{1/2}\}. \tag{27}$$

The important parameter here is F_0, the grid surface required to make the SGS fluxes equal to the total turbulent fluxes. The coefficients c_{10} and c_{T10} are correction factors which have been adjusted numero-empirically; the coefficient c_{T10} depends also on the molecular Prandtl number.

The Subgrid Scale Kinetic Energy Transport Equation

The SGS kinetic energy ${}^{v}\overline{E'} = \frac{1}{2}\,{}^{v}\overline{(u_i - {}^{v}\overline{u}_i)^2}$ is calculated integrating an additional transport equation as described in [2]. The following changes and extensions have been introduced [4].

The production term, Eqs. (24) and (36) of [2], has been extended to include the SGS energy production caused by the inhomogeneous part of the SGS stresses. This change has

been found to be important in the near-wall region, especially in annular channels, in order to predict a correct cross-stream energy profile.

The dissipation rate ϵ is now modeled by means of three terms: $\epsilon = \epsilon_I + \epsilon_{II} + \epsilon_{III}$. The first term replaces the old model (c_3 as in [2]):

$$\epsilon_I = c_3(\overline{v'E'})^{3/2}/\min(h, c_{31}\ell). \tag{28}$$

The inclusion of the minimum function makes the model suited for very coarse grids, in particular near the walls, where the mixing length ℓ becomes smaller than the mesh scale h. For small Reynolds numbers it has been found to be necessary to add the second term, which describes the direct viscous dissipation:

$$\epsilon_{II} = \nu\, c_{32}\, \overline{v'E'}/[\min(h, c_{31}\ell)]^2. \tag{29}$$

The values of c_{31} and c_{32} have been determined [4] from the empirical energy spectra proposed by *Pao* [7]. According to *Jones* and *Launder* [8], finally the term

$$\epsilon_{III} = 2\nu\,[\delta_3(\overline{v'E'})^{1/2}]^2 \tag{30}$$

has been added, which accounts for the dissipation in the viscous sublayer. It is of negligible magnitude, however, for those Reynolds numbers and mesh sizes considered up to now. The relative magnitude of these three dissipation terms is shown in Fig. 3 for two examples.

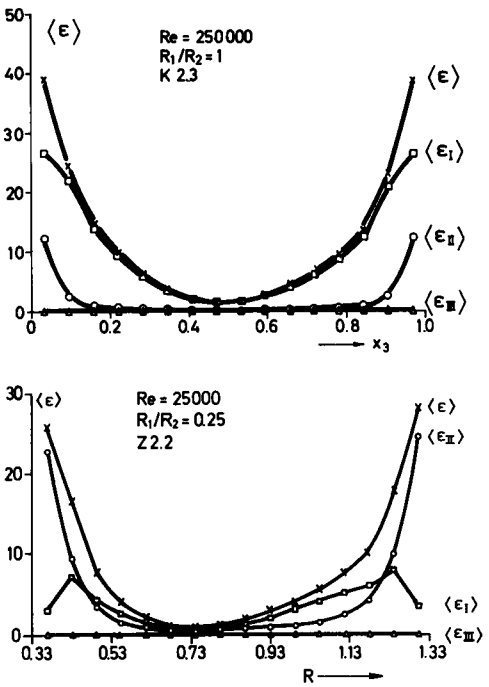

Fig. 3. Energy dissipation rate $\langle\epsilon\rangle$ and its three parts for two cases, K 2.3 and Z 2.2

Table 2. Case specifications

	K7	*K2.2*	*K2.3*	*Z2.2*
X_1	2	3.2	4	3.2
X_2	1	2	2	π
IM	16	32	64	32
JM	8	16	32	32
KM	16	16	16	16
R_1/R_2	1	1	1	0.25
Re	18,700	25,000	250,000	25,000
Pr	0.71	0.007	0.7	0.7
CPU-time IBM 370/168	40 min	3 h	18 h	7 h
Problem time	6.05	4.24	4.23	4.51
No. of time Steps	2,128	2,350	3,224	2,625

The Boundary Conditions

In the x_1- and x_2-direction we assume periodicity with periodic lengths X_1 and X_2 (or angle, resp.), the values of which are listed in Table 2.

In the x_3-direction, at the walls we set the normal velocity to zero. In addition, the no-slip boundary condition requires prescription of the wall shear stresses $\tau_{wi} = -\nu \overline{\frac{\partial u_i}{\partial x_3}}^{3}$ and the normal wall heat flux $\dot{q}_w = -a \overline{\frac{\partial T}{\partial x_3}}^{3}$ as a function of the velocities and temperatures in the wall adjacent grid cells. The stresses are computed as in [2] with two important changes [4] which refer to Eq. (45) of [2]. First, the time mean value $\langle \tau_w \rangle$, which is equal to 1 in the present units for a steady-state plane channel flow, is not prescribed this way rather than recalculated by proper averaging from the actual and recent velocity fields. Secondly, the wall roughness coefficient E can be a function of the equivalent sand-roughness height and the x_2-coordinate. This allows us to study secondary flows. The boundary condition in terms of the heat flux $\dot{q}_w$ is approximated for small Peclet numbers by

$$\dot{q}_w = -\frac{a}{\Delta x_3/2} ({}^{v}\overline{T}_1 - T_w). \tag{31}$$

(${}^{v}\overline{T}_1$ = first grid cell value, T_w = wall temperature). For large Peclet numbers we use

$$\dot{q}_w = \langle \dot{q}_w \rangle ({}^{v}\overline{T}_1 - T_w)/\langle {}^{v}\overline{T}_1 - T_w \rangle \tag{32}$$

where either $\langle \dot{q}_w \rangle$ or T_w must be prescribed and the unknown part is determined from the logarithmic law of the wall [9] averaged over the first grid cell

$$\langle {}^{v}\overline{T}_1 - T_w \rangle = -\frac{\langle \dot{q}_w \rangle}{\langle \tau_w \rangle^{1/2}} \frac{1}{\kappa_H} [\ln(\mathrm{Re}_\tau \langle \tau_w \rangle^{1/2}) + \ln(\Delta x_3) - 1] + B_T \tag{33}$$

($\kappa_H = 0.465$, B_T = function of wall roughness and Prandtl number [4]).

By setting $u_3^{n+1} = 0$ at the walls, instead of using (12), the Neumann boundary condition $\delta_3 p = 0$ at the wall follows from (15).

Results

The purpose of this chapter is to demonstrate the general agreement between experiments and TURBIT-2 results.

SGS Model Sensitivity

Several preliminary cases have been run in order to study the effect of the free SGS parameters σ_1, σ_T, c_{10}, and c_{T10}, The values of which can be estimated to be of order one theoretically but remain to be fixed numero-empirically. For this purpose a rather coarse grid has been used (K 7, see Table 2). Typical results [4] are a 15% increase of the kinetic energy near the walls (which is the most sensitive measure) as a result of a 20% increase of σ_1 and a 5% decrease of the same quantity as a result of a 10% increase of c_{10}. As shown in Fig. 4, the importance of the temperature model coefficients σ_T and c_{T10} are smaller. The values finally used are those listed in Tab. 1. One should be reminded that an even weaker sensitivity is observed for finer grid resolutions.

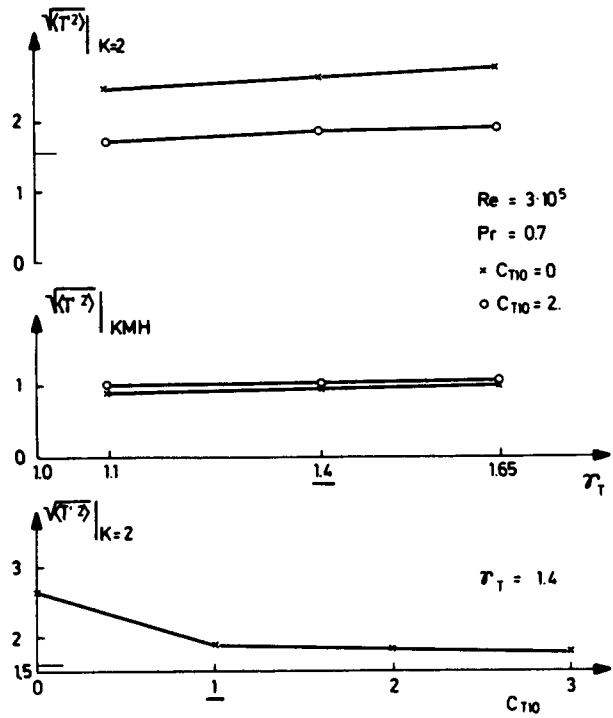

Fig. 4. rms temperature fluctuations in the radial cells at $K = 2$ and $K = KMH = KM/2$ (channel middle) as a function of the SGS coefficients, case $K7$

Flow Field and Velocity Statistics

Figure 5 shows a typical resulting turbulent flow field for case $Z2.2$. This is an annulus ($R1/R2 = 0.25$) heated from the inner rod with an adiabatic outer wall. The contour lines and velocity vectors show the known quasi-random behavior. The flow is from left to right. The velocity contour lines show some inclination against the flow direction towards the channel middle; this is observed in all plots of this type. The fluctuating kinetic energy is generally a rather smooth space-function except for some peaks (bursts?) near the walls, which are mainly

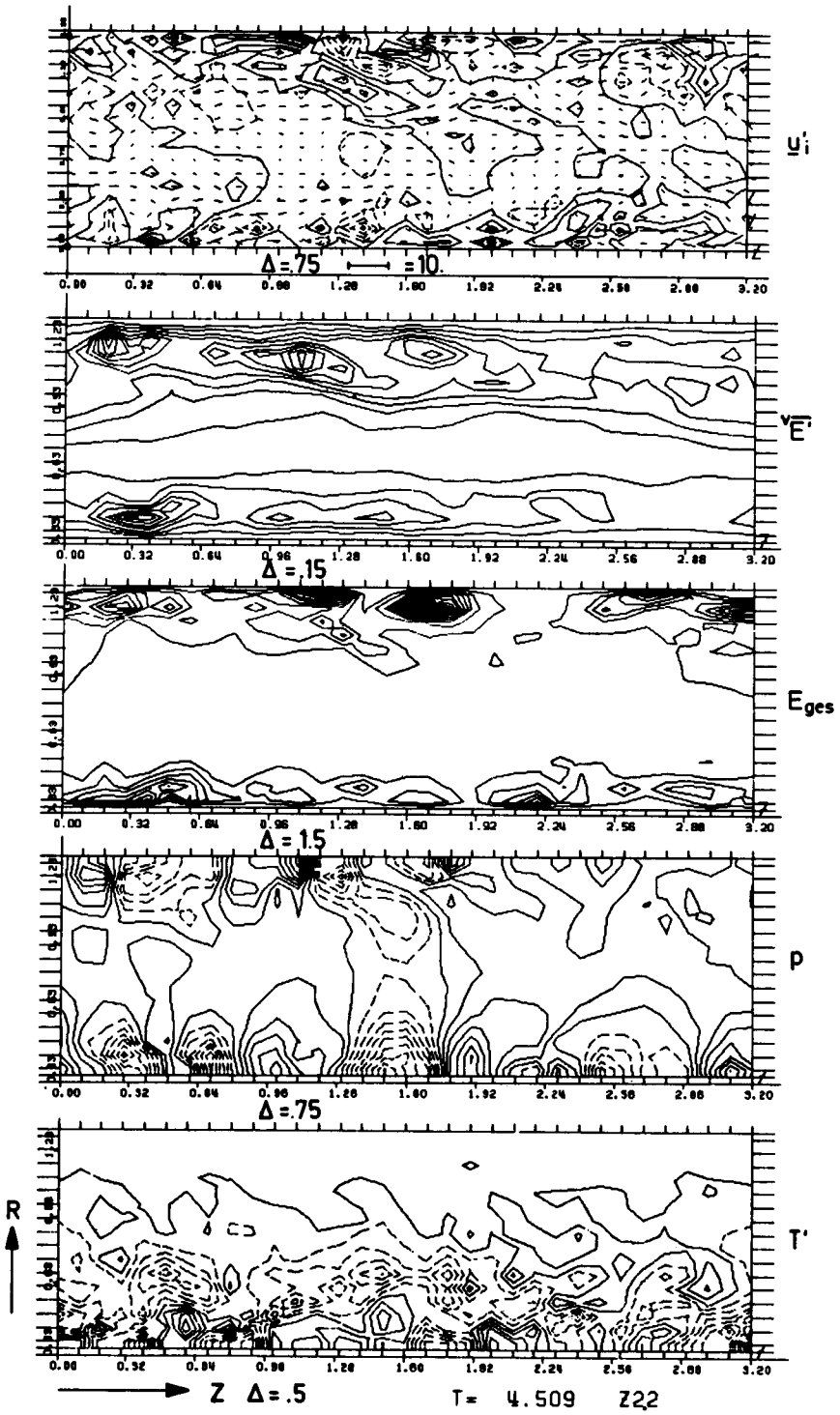

Fig. 5. Vector- and contour-line plots of the instantaneous resolved fluctuating velocities $u_i' = u_i - \langle u_i \rangle$, SGS kinetic energy $\overset{v}{\overline{E'}}$, total energy $E_{ges} = \overset{v}{\overline{E'}} + u_i'^2/2$, fluctuating pressure p and temperature T' in an annulus (Z 2.2). Δ = contour line increment, dashed curves correspond to negative values

contained in the directly resolved part of the flow field. As expected from experiments [10, 11], the kinetic energy is larger near the outer wall than near the inner one. This result was not so obvious in the older code-version [3]. The temperature fluctuations are large near the heated inner wall only.

The time mean value of the kinetic energy is shown in Fig. 6. Also plotted in this figure is the SGS part which amounts to less than 25% of the total value. The corresponding dissipation rates are depicted in Fig. 3 mentioned above. Here we see the effect of the three model parts for two different Reynolds numbers. The direct viscous dissipation rate ϵ_{II} is not negligible especially near the walls. The computed velocity profile given in Fig. 7 shows very good agreement with the corresponding experimental results of *Ball* [12] and *Lee* [13]. The difference between the measured and computed maximum value $\langle u_{1\,max} \rangle$ itself is less than 1% if we refer to *Lee*. The results of *Ball* are smaller by 10%, this seems to be a consequence of rather densely located spacers used by *Ball* in his annular channel. Figure 8 shows the shear stress; the smaller values correspond to that part of the shear stress resolved directly by the large-scale flow. We conclude that the major part of the momentum transport is accomplished by the resolved flow part. No experimental data are available for this ratio of radii. We have included some measurements for other radii to show the general agreement.

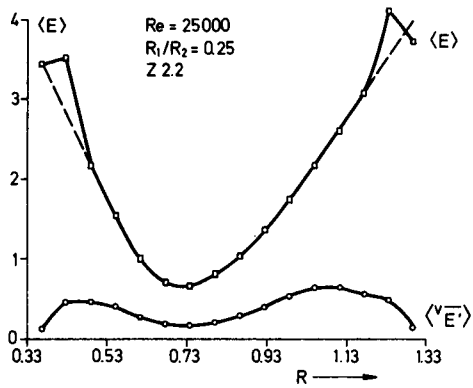

Fig. 6. Total ($\langle E \rangle$) and SGS ($\langle \overline{{}^{v}E'} \rangle$) kinetic energy

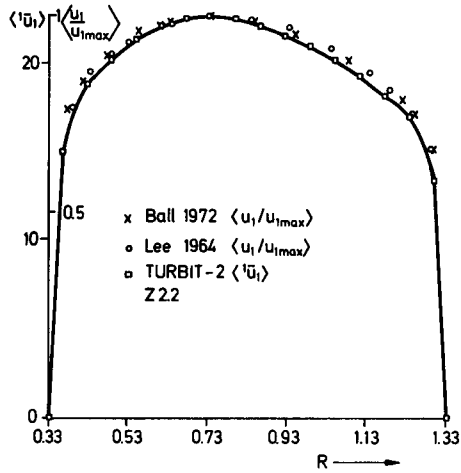

Fig. 7. Time mean velocity profile

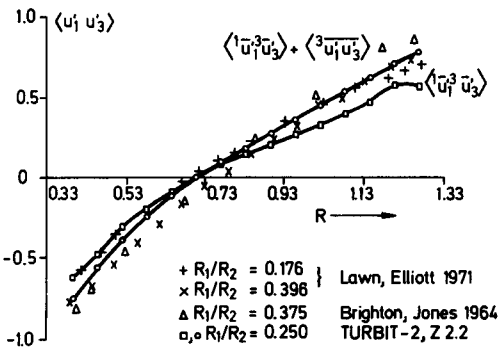

Fig. 8. Total and large-scale turbulent shear stress

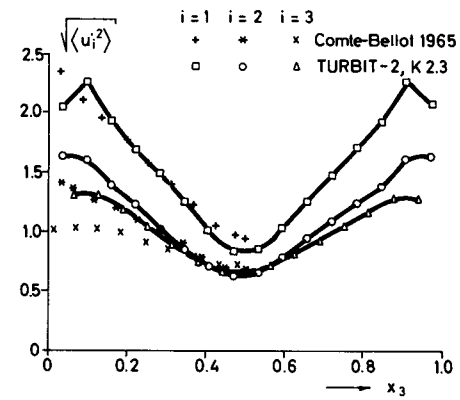

Fig. 9. rms velocity fluctuations

For a plane channel we compare our computed rms velocity fluctuations with the measured results of *Comte-Bellot* [14] (see Fig. 9). The differences are less than about 20%. Some of the differences might be attributable to the SGS part which has been computed from the SGS kinetic energy and added to the resolved part under the assumption of local isotropy. In all our simulations we observe a surprising result: The u_3 rms values are larger than the u_2 values by a few percent in the middle of the channel. This might be a consequence of anisotropy and different resulting energy supply to these velocity components by means of the pressure fluctuations. It is not clear from experiments whether this effect is real, because the accuracy of the measurements is not sufficient for this purpose. Interestingly, this result is not discordant with the measurements of *Comte-Bellot* [14].

Pressure Statistics

The time mean value of the pressure is not a constant as shown in Fig. 10. Using an arbitrary mean value (the mean is set to zero in the first cell near the left wall by the Poisson-solver used), we compare our computations with the experiments of *Patterson* et al. [15]. The rms pressure fluctuations are plotted in Fig. 11. The rms value at the wall, 2.7, corresponds well with experiments [3]. No internal measurements are known for this geometry. The case $K7$ gives rather small rms values, this is a consequence of too small periodicity lengths X_1 and X_2, which result in a filtering of the low-frequency fluctuations.

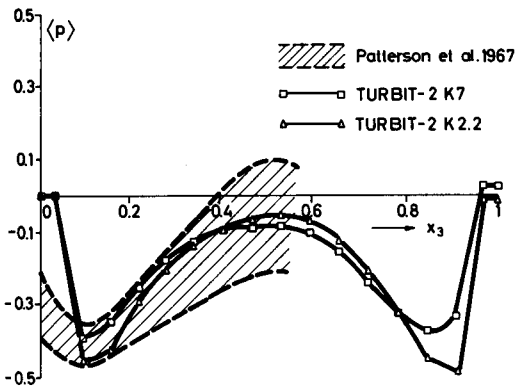

Fig. 10. Time mean pressure profile

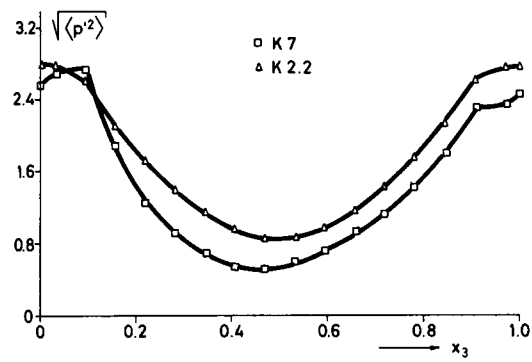

Fig. 11. rms pressure fluctuations

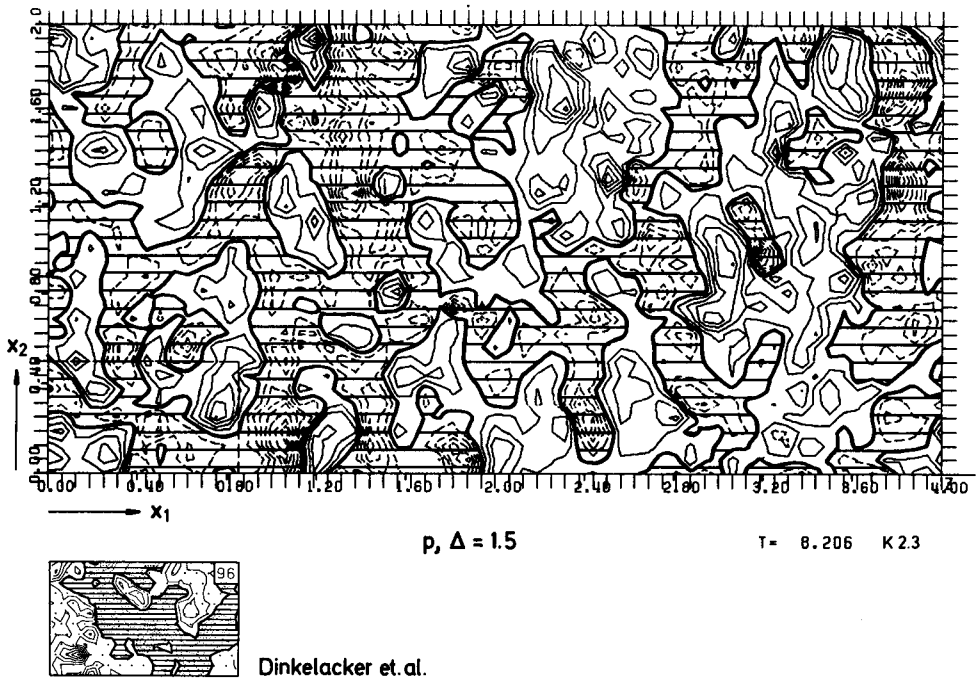

Fig. 12. Instantaneous pressure fluctuations at the wall computed (above, case $K2.3$) and measured [17] (left). The dashed regions contain negative fluctuations

Figure 12 shows a contour-line plot of the instantaneous fluctuating pressure at the wall of a plane channel ($K2.3$) and the corresponding experimental result of *Dinkelacker* et al. [16, 17]. Both plots are scaled so that the spatial dimensions are directly comparable. In both figures we observe a 45°-inclination. From the numerical results it is obvious that the pressure fluctuations are correlated over longer distances in the x_2-direction than in the mean flow direction x_1. This finding agrees with earlier results [3] and experiments [18]. The convective velocities of the wall pressure fluctuations are roughly the bulk velocity [19].

Temperature Statistics

The mean temperature profile, corresponding to Fig. 5 ($Z2.2$) is shown in Fig. 13. The agreement with experimental data [12, 13, 20] is satisfactory except for the results of *Ball*, which depart probably due to the above mentioned spacers and a rather short thermal entry length. The Nusselt-number, calculated from this mean temperature profile, is Nu = 50.6. Experimental results deviate from this value by ± 15% [4].

For a plane channel with a rather coarse grid ($K7$), we show the rms temperature fluctuations in Fig. 14. In this case the fluid is heated by a volumetrical heat source within the fluid and cooled at both walls by prescribing constant and equal wall temperatures. No equivalent experimental data are known for a plane channel. We, therefore, refer to the pipe data of *Bremhorst* et al. [21], which are in reasonable agreement. Caused by the deficiencies of the experimental equipment, the data of Bremhorst are 15% too small [22]. In Fig. 15 we show the correlation coefficient between the temperature component and the cross-stream velocity component for the same channel in comparison to several experiments [21–25]. The good agree-

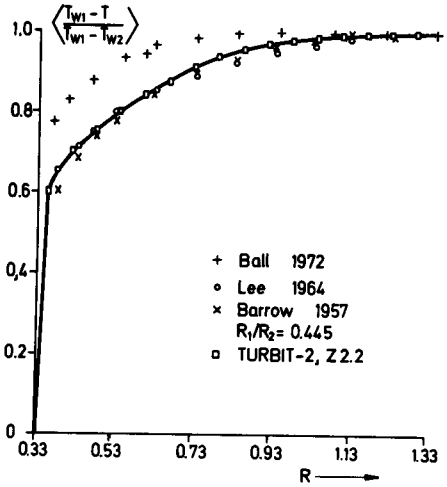

Fig. 13. Time mean temperature profile normalized by the wall temperatures at the inner and outer walls (T_{w_1}, T_{w_2})

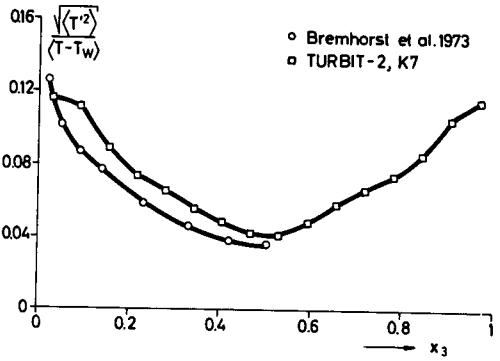

Fig. 14. rms temperature fluctuations. The experimental results are for a pipe flow [21]

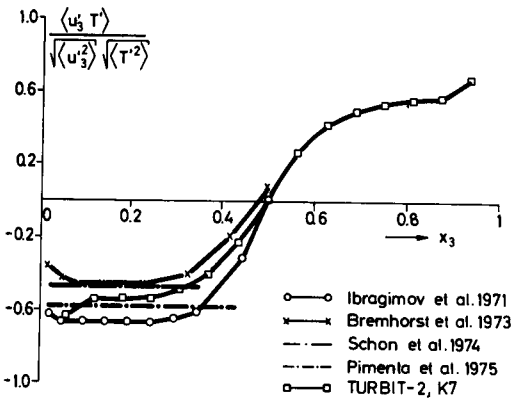

Fig. 15. Cross-stream velocity-temperature correlation coefficient

ment shows that the turbulent heat flux is correctly simulated. This is mainly a consequence of the inhomogeneous part (16, 19) of the SGS heat-flux model; it was found [4] that neglection of the inhomogeneous SGS heat-flux model results in higher temperature rms values (see Fig. 4), which cause smaller turbulent heat-flux correlation coefficients. Further results with respect to varying molecular Prandtl numbers and resulting turbulent Prandtl numbers [4, 26] have been obtained. Also, secondary flows induced by varying wall roughness have been observed numerically [27].

Conclusions

Our main conclusion is that TURBIT-2 is a well-suited code to simulate directly turbulent velocity and temperature fields in channel flows even if rather poorly resolving grids are used. This result is a consequence of several improvements which have been added to the SGS model.

In particular, the SGS kinetic energy equation and the inhomogeneous part of the flux approximations have been improved.

It has been shown that the resulting temperature fields are rather insensitive with respect to the model coefficients. The differences between the numerical results and experimental data are small in comparison with the scatter of the latter.

We are now able to produce results which can hardly be measured like, e.g., the pressure statistics and pressure-temperature correlations, using only a modest amount of computing time (e.g., 40 minutes for case $K7$). This achievement has to be payed for, however, by a small increase in empirical information required; also, the amount of novel information extractable from a direct simulation decreases with decreasing resolution.

References

1. Deardorff, J. W., "A numerical study of three-dimensional turbulent channel flow at large Reynolds numbers", J. Fluid Mech. *41*, 453–480 (1970)
2. Schumann, U., "Subgrid scale model for finite difference simulations of turbulent flows in plane channels and annuli", J. Comput. Phys. *18*, 376–404 (1975)
3. Schumann, U., "Numerical investigation of the wall pressure fluctuations in channel flows", Nucl. Eng. Des. *32*, 37–47 (1975)
4. Grötzbach, G., "Direkte numerische Simulation turbulenter Geschwindigkeits-, Druck- und Temperaturfelder in Kanalströmungen", Thesis, KFK 2426 (University of Karlsruhe 1977)
5. Schumann, U., "Ein Verfahren zur direkten numerischen Simulation turbulenter Strömungen in Platten- und Ringspaltkanälen und über seine Anwendung zur Untersuchung von Turbulenzmodellen", Thesis, KFK 1854 (University of Karlsruhe 1973)
6. Lörcher, G., "Laser-Doppler-Messungen von Energiedichtespektren in turbulenter Kanalströmung", Thesis, KFK 2448 (University of Karlsruhe 1977)
7. Pao, Y. H., "Structure of turbulent velocity and scalar fields at large wave numbers", Phys. Fluids *8*, 1063–1075 (1965)
8. Jones, W. P., and Launder, B. E., "The calculation of low Reynolds-number-phenomena with a two-equation model of turbulence", Int. J. Heat Mass Transfer *16*, 1119–1130 (1973)
9. Kader, B. A., and Yaglom, A. M., "Heat and mass transfer laws for fully turbulent wall flows", Int. J. Heat Mass Transfer *15*, 2329–2351 (1972)
10. Brighton, J. A., and Jones, J. B., "Fully developed turbulent flow in annuli", J. Basic Eng. *86*, 835–844 (1964)
11. Lawn, C. J., and Elliott, C. J., "Fully Developed Turbulent Flow Through Concentric Annuli", CEGB-Report RD/B/N 1878 (1971)
12. Ball, H. D., "Experimental Investigation of Eddy Diffusivities of Air in Turbulent Annular Flow", Ph. D. Thesis (Kansas State University 1972)
13. Lee, Y., "Turbulent Flow and Heat Transfer in Concentric and Eccentric Annuli", Ph. D. Thesis (University of Liverpool 1964)
14. Comte-Bellot, G., "Ecoulement turbulent entre deux parois parallèles", Publ. Sci. Tech. Minist. Air Fr. *419* (1965)
15. Patterson, G. K., Ewbank, W. J., and Sandborn, V. A., "Radial pressure gradient in turbulent pipe flow", Phys. Fluids *10*, 2082–2084 (1967)
16. Dinkelacker, A., Hessel, M., Meier, G. E. A., and Schewe, G., "Further Results on Wall Pressure Fluctuations in Turbulent Flow", Federal Republic of Germany Hydroacoustics Symposium, ed. by H. Merbt, Vol. 3 (Frauenhofer Ges., München 1975) pp. 29–38
17. Dinkelacker, A., Hessel, M., Meier, G. E. A., and Schewe, G., "Investigation of Pressure Fluctuation Beneath Turbulent Boundary Layer by Means of an Optical Method", Bericht 105 (Max-Planck-Institut für Strömungsforschung, Göttingen 1977)
18. Clinch, J. M., "Measurement of the wall pressure field at the surface of a smooth-walled pipe containing turbulent water flow", J. Sound Vib. *9*, 398–419 (1969)
19. Grötzbach, G., "Convective Velocities of Wall Pressure Fluctuations in a Turbulent Channel Flow Deduced from a Computer-Generated Movie", in *Structure and Mechanisms of Turbulence II*, ed. by H. Fiedler, Lecture, Notes in Physics Vol. 76 (Springer, Berlin, Heidelberg, New York 1978), 320–324

20. Barrow, H., "Fluid Flow and Heat Transfer in an Annulus with a Heated Core Tube", Proc. Inst. Mech. Eng. London *169*, 1113–1124 (1957)
21. Bremhorst, K., and Bullock, K. J., "Spectral measurement of turbulent heat and momentum transfer in fully developed pipe flow", Int. J. Heat Mass Transfer *16*, 2141–2154 (1973)
22. Bremhorst, K., personal communication (1977)
23. Ibragimov, M. Kh., Subbotin, V. I., and Taranov, G. S., "Velocity and temperature fluctuations and their correlations in the turbulent flow of air in pipes", Int. Chem. Eng. *11*, 659–665 (1971)
24. Schon, J. F., Mathieu, J., Baille, A., Solal, J., and Comte-Bellot, G., "Experimental study of diffusion processes in unstable stratified boundary layers", Adv. Geophys. *18B*, 265–272 (1974)
25. Pimenta, M. M., Moffat, R. J., and Kays, W. M., "The Turbulent Boundary Layer: An Experimental Study of the Transport of Momentum and Heat with the Effect of Roughness", Report HMT-21 (Stanford University 1975)
26. Grötzbach, G., "Erste Ergebnisse der direkten numerischen Simulation von Temperaturfeldern bei turbulenter Natriumströmung", KFK 1276/2, 129–6 – 129–11 (Kernforschungszentrum Karlsruhe 1976)
27. Grötzbach, G., "Direct Numerical Stimulation of Secondary Currents in Turbulent Channel Flows", in *Structure and Mechanisms of Turbulence II*, ed. by H. Fiedler, Lecture Notes in Physics Vol. 76 (Springer, Berlin, Heidelberg, New York 1978), 308–319

Reprint from

Turbulent Shear Flows I

Editors: F. Durst B. E. Launder F. W. Schmidt J. H. Whitelaw

Springer-Verlag
Berlin Heidelberg New York